Published online 16 February 2017

Nucleic Acids Research, 2017, Vol. 45, No. 9 ***5449–5457***
doi: 10.1093/nar/gkx063

Self-assembly of multi-stranded RNA motifs into lattices and tubular structures

Jaimie Marie Stewart[1], Hari K. K. Subramanian[2] and Elisa Franco[2,*]

[1]Department of Bioengineering, University of California, 900 University Avenue, Riverside, CA 92521, USA and
[2]Department of Mechanical Engineering, University of California, 900 University Avenue, Riverside, CA 92521, USA

Received May 19, 2016; Revised December 30, 2016; Editorial Decision January 23, 2017; Accepted January 31, 2017

ABSTRACT

Rational design of nucleic acid molecules yields self-assembling scaffolds with increasing complexity, size and functionality. It is an open question whether design methods tailored to build DNA nanostructures can be adapted to build RNA nanostructures with comparable features. Here we demonstrate the formation of RNA lattices and tubular assemblies from double crossover (DX) tiles, a canonical motif in DNA nanotechnology. Tubular structures can exceed 1 μm in length, suggesting that this DX motif can produce very robust lattices. Some of these tubes spontaneously form with left-handed chirality. We obtain assemblies by using two methods: a protocol where gel-extracted RNA strands are slowly annealed, and a one-pot transcription and anneal procedure. We identify the tile nick position as a structural requirement for lattice formation. Our results demonstrate that stable RNA structures can be obtained with design tools imported from DNA nanotechnology. These large assemblies could be potentially integrated with a variety of functional RNA motifs for drug or nanoparticle delivery, or for colocalization of cellular components.

INTRODUCTION

Self-assembled nucleic acid nanostructures are becoming increasingly important in therapeutic applications and synthetic biology because they serve as programmable, versatile scaffolds to organize an ever expanding variety of ligands (1,2). RNA scaffolds present several advantages relative to DNA: they can be transcribed in large amounts (3,4), can naturally include functional domains that are exclusive to RNA (5) and present better immune compatibility relative to DNA (6) for transfection and delivery of molecular cargo.

While existing RNA assembly methods allow the generation of a variety of nanoscale structural and functional motifs, the size of assemblies that have robust, periodic nanoscale features remains limited. While loose filamentous assemblies (7–9) as well as arrays with loose lattice structures (10–12) can reach microns in size, well-defined RNA periodic lattices reach at most a few hundred nanometers (nm) (4). This limitation is not present in DNA nanotechnology: micron-sized, highly regular assemblies with up to tens of thousands of nucleotides (nt) have been demonstrated (13–15). In particular, multi-stranded DNA tiles that bind via rationally designed Watson–Crick (WC) complementary domains yield a variety of large arrays and tubular structures that can grow up to tens of microns in length (13,16). These structures are compatible with decoration with a variety of organic and inorganic ligands, resulting in heterogeneous materials with the capacity for scalable growth and even algorithmic assembly (17–19).

Large DNA nanostructures are multi-stranded architectures where helices are held together by Holliday junctions, and sequence content is rationally optimized (20,21). In contrast, RNA assemblies (both nanoparticles and tiling systems) are generally designed by exploiting conserved tertiary motifs such as kissing loops (4,10,22) or pRNA multimers (23,24). Although successful in the construction of sophisticated two- and three-dimensional objects, this approach has so far yielded structures of limited size and it relies on a restricted sequence design space. Additionally, assemblies held together by tertiary structure motifs may not be easily compatible with toehold-mediated branch migration (25), a powerful mechanism to obtain dynamic control of self-assembly in DNA circuits and nanostructures (26,27). DNA design methods can in principle be adapted to build assemblies with RNA by taking into account the A-form geometry of the RNA duplex (11 bp helical pitch and ≈20° base inclination). This strategy was used to build nanoscale multi-stranded objects (3,28), multi-stranded DNA–RNA hybrid structures (29,30), small RNA origami structures (31) and assemblies from single-stranded tiling systems (4). These results suggest that this route could be pursued to build large, multi-stranded architectures solely of RNA.

Here we demonstrate that multi-stranded RNA double crossover (DX) tiles assemble into large arrays and tubular structures, which can exceed 1 μm in size. RNA structure as-

*To whom correspondence should be addressed. Tel: +1 951 827 2442; Fax: +1 951 827 3188; Email: efranco@engr.ucr.edu

sembly is characterized by gel electrophoresis, atomic force microscopy (AFM) and transmission electron microscopy (TEM). We find that assembly correctness and yield are affected not only by tile sequence content but also by nick position on the tile helices. We find that some of the tubular structures are chiral and can be interpreted as left-handed (none of the tubes can be unambiguously interpreted as right-handed). Assemblies are obtained with two distinct protocols; one where RNA strands are annealed after individual gel extraction, and one where RNA components are simultaneously transcribed and subsequently annealed without gel extraction.

MATERIALS AND METHODS

Oligonucleotides

RNA strands were transcribed from DNA templates with a T7 promoter; DNA template sequences are reported in the Supplementary Information File (SI) Section 1. DNA strands were purchased from Integrated DNA Technologies (Coralville, IA, USA). Concentrations of nucleic acids were determined by absorption measurements (Nanodrop 2000c, Thermo Scientific).

RNA sequences for Design 1 are:

- Sa1: 5′-GGUGCGACUAUGCAACCUGCCUGGC AAGACCUACGAUGGACACGGUAACG,
- SbR1: 5′-GUCUUG CCAGGCACCAUCGUAGGUC UUGCCAGGCACCAUCGUAG,
- SbC1: 5′-CAGAAAUUAACUAAAGAAGCGGCAG AAAUUAACUAAAGAAGCGG,
- SbL1: 5′-GAAAUUAACUAAAGAAGCGGCAGAA AUUAACUAAAGAAGCGGCA,
- Sc1: 5′-GCACCCGUUACCGUGUGGUUGCAUA GUC.

RNA sequences for Design 2 are:

- SbR2: 5′-GGCAGAAAUUAACUAAAGAAGCGGC AGAAAUUAACUAAAGAAGC,
- SbC2: 5′-CAGAAAUUAACUAAAGAAGCGGCAG AAAUUAACUAAAGAAGCGG,
- SbL2: 5′-GAAAUUAACUAAAGAAGCGGCAGAA AUUAACUAAAGAAGCGGCA,
- Sc1: 5′-GGACCAAGAUAGAAUGAGUUGAAGU AUA.

The complete list of strands used and sequence diagrams for each tile can be found in SI Section 1, 2 and in Supplementary Figure S1. Additional details for all the experimental protocols can be found in SI section 3.

RNA extraction

Purified RNA strands were individually transcribed *in vitro* using the AmpliScribe T7-Flash transcription kit (#ASF3507 Epicenter, Inc.) from corresponding DNA templates (SI file Section 1). RNA strands were gel extracted by either 10% or 15% denaturing polyacrylamide gel electrophoresis (PAGE). Next, RNA was eluted using 0.3 M sodium acetate at pH 5.3. Finally, RNA was precipitated using ethanol and glycogen. Additional details are provided in the SI file Section 3.5.

Polyacrylamide gel electrophoresis (PAGE)

Denaturing PAGE. A gel pre-mix was prepared by mixing urea, nanopure water, acrylamide/bis-acrylamide 19:1, 40% solution, which was heated until the urea completely dissolved. To start polymerization, the pre-mix was mixed with Tris-Borate-EDTA (TBE) buffer, ammonium persulfate (APS) and Tetramethylethylenediamine (TEMED) and nanopure water in the appropriate amounts. Gels were cast in 10 × 10 cm, 1 mm thick mini gel cassettes (Thermo Scientific, #NC2010) and allowed to polymerize for at least 2 h before electrophoresis. Gels ran at room temperature at 100V in 1× TBE unless otherwise noted. After electrophoresis the gels were stained with SYBR® Gold Nucleic Acid Gel Stain (Invitrogen, #S11494) for 20–30 min; gels were imaged using the Biorad ChemiDoc MP system.

Non-denaturing PAGE. Acrylamide/bis-acrylamide 19:1, 40% solution, Tris-acetate-EDTA (TAE), Magnesium Chloride ($MgCl_2$), APS and TEMED were added together at appropriate concentrations for the desired polyacrylamide percentage, then cast in 10 × 10 cm, 1 mm thick mini gel cassettes (Thermo Scientific, #NC2010) and allowed to polymerize for at least 2 h before use. Gels ran at 4°C at 150 V in 1× TBE buffer. After electrophoresis gels were stained with SYBR® Gold Nucleic Acid Gel Stain (Invitrogen, #S11494) for 20 min then imaged using the Biorad ChemiDoc MP system.

Agarose gel electrophoresis

We prepared 0.5% high-melt agarose gels (made using Bio-Rad Certified Megabase Agarose, Cat No:1613108) in 1× TBE and 6 mM $MgCl_2$ by heating 0.5 g of Agarose in 100 ml of the buffer. Ethidium Bromide was added at 0.5 μg/ml concentration to the mix prior to casting the gel (Owl Easy-cast B1 gel system, 9 × 11 cm—Thermo Scientific). After loading the samples, wells were sealed using thin films of solid agarose affixed on top of the wells using molten agarose, to reduce the loss of assemblies too large to enter the gel matrix. Running buffer also contained Ethidium Bromide at 0.5 μg/ml concentration. The gel was run at room temperature at 60 V for 2.5 h. Gel images were taken using a BioRad ChemiDoc MP gel imaging system.

Assembly of RNA structures

Gel extracted and annealed strands. Each RNA strand was individually transcribed, gel extracted and purified as described earlier. Then, strands Sa, Sb and Sc were added in a 2:1:2 ratio (required stoichiometry to form a single tile) to a solution of 1× TAE and 12.5 mM $MgCl_2$. This mix was slowly annealed from 70 to 22°C over 24 h. The final tile concentration for this protocol was 500 nm, unless otherwise noted (e.g. to anneal tile D1R we mixed 1 μm Sa1, 500 nm SbR1 and 1 μm Sc1). Annealed samples were directly imaged (AFM or TEM) or electrophoresed.

One-pot transcribed and annealed strands. For the one pot assembly, the three templates transcribing tile RNA strands were added in a 2:1:2 ratio (Sa:Sb:Sc) to a solution of 1× TAE, 22.5 mM $MgCl_2$, 2.25 mM of each Nucleoside triphosphates (NTP), 10 mM Dithiothreitol and 1/6 volume dilution of AmpliScribe T7-Flash Enzyme Solution (Epicentre, # ASF3507). Unless otherwise noted, the quantity of templates added to each sample was 1:0.5:1 μg (Sa:Sb:Sc), in a total reaction volume of 20 μl. The solution was then allowed to incubate at 37°C for 15 min, then immediately annealed from 70 to 22°C over 24 h. The quantity of templates added was tuned by changing it by ±0.5 μg, while maintaining their ratios.

AFM imaging

AFM images were obtained in tapping mode under buffer using a Digital Instruments Multimode AFM with a Nanoscope (R) III controller. Bruker SNL-10 silicon tip on a nitride lever with a spring constant of ≈ 0.24 N/m were used for imaging, with a drive frequency of ≈ 9–10 kHz. AFM buffer consisted of the same buffer used for annealing unless otherwise noted.

TEM imaging

TEM images were obtained using a FEI Tecnai12 operated at 120 kV (single tilt holder, Gatan US1000 digital CCD camera). TEM grids were glow discharged using a Cressington Coating System. A total of 5 μl of sample was placed on parafilm, the TEM grid was placed copper side down on sample for 5 min. Excess sample was carefully wicked away. The grid was then rinsed, by placing the grid copper side down on a droplet of deionized water for 5 min; excess liquid was wicked away and the grid was rinsed once more using this method. Excess liquid was removed with Whatman paper. Grid was then placed copper side up and 5 μl of 1% uranyl acetate was added and allowed to stain for 30 s.

RESULTS

Design of RNA tiles

RNA tiles were designed according to one of the DX motifs proposed by Ko *et al*. (29) to build DNA–RNA hybrid tiles, because DNA–RNA duplexes are expected to have A-form geometry as RNA–RNA duplexes. Some of the DNA–RNA hybrid motifs used by Ko *et al.* resulted in tubular structures, so we reasoned that by importing the same motifs we could build RNA nanotubes.

As shown in Figure 1A, three unique RNA strands (Sa, Sb, Sc) are designed to have WC complementary domains that interact forming five-stranded tiles, where two helices are held together by two four-way antiparallel Holliday junctions, or crossovers (hence the DX nomenclature); the intra-tile crossover distance is 22 base pairs (bp) or two full RNA helical turns (in comparison, 21 bases result in two full DNA helical turns). These DX tiles are therefore similar to the Double crossover, Anti-parallel, Even number of half-turns between both inter-tile and intra-tile crossovers (DAE-E) DNA tile motif (13,32). Taking as a reference the tile schematic in Figure 1A, the position of the nick in strand Sb was chosen to be centered (SbC), two base pairs to the right (SbR) or two bases to the left (SbL) of the crossover midpoint. Tiles interact via 5 (nt) long overhangs or sticky-ends, whose complementarity is depicted in the gray tile abstraction in Figure 1A. A Chimera (33) rendering of this tile motif with right-positioned nick is in Figure 1B. The inter-tile crossover distance is 28 nt (Figure 1C). Because this distance is close to 2.5 turns (29 nt), adjacent tiles are expected to assemble in a face-up (O-marked tile in Figure 1C), face-down pattern (X-marked tile) which should yield flat lattices. Yet in (right-positioned nick) hybrid DNA–RNA tiles (29) an inter-tile crossover distance slightly deviating from exactly 2.5 turns appears to promote formation of tubular structures. An example AFM image of assembled RNA tiles is shown in Figure 1D.

Because sequence content can affect the yield and stability of nucleic acid assemblies, we tested two different sets of sequences for the same tile motif in Figure 1A. The first set of sequences, indicated as D1, was chosen by converting to RNA the sequences in Ko *et al.* (29), which were originally identified using Sequin (34). Design D1 includes variants D1R, D1C and D1L where the nick position in strand Sb is changed according to Figure 1A (while strands Sa1 and Sc1 are unchanged). Additionally, we considered variant D1RE: this variant includes a 5 nt single stranded overhang on the 5′ end of strand Sa1 (Supplementary Figure S22). A second set of sequences, D2, was chosen using the DNA Design Toolbox (35,36) (built on the Vienna RNA package (37)), by writing a computer script that requires the minimization of unwanted secondary structures at 37°C. The absence of secondary structure in each strand of D2 at 37°C was confirmed using NUPACK (20). Design D2 includes variants D2R, D2C and D2L, where only the nick position in strand Sb is varied.

RNA molecules were transcribed from linear templates under control of the T7 bacteriophage promoter; all sequences are reported in the SI. Because transcription yield is significantly reduced in the absence of at least two G nucleobases after the +1 promoter position, we incorporated this constraint when designing sequences for tile D2R.

Assembly methods

RNA nanostructures are typically assembled using post-transcription procedures that include gel extraction and thermal annealing treatments (10,28) to eliminate transcripts of incorrect length and misfolded strands. Thus, in our first set of experiments individual strands of tiles D1R and D2R were transcribed, gel-extracted, mixed at appropriate stoichiometry in TAE and 12.5 mM $MgCl_2$ buffer, heated to 70°C and cooled to room temperature over 24 h (29) (Figure 2A).

In Figure 2B and C we show AFM images of this gel-extraction self-assembly protocol for tiles D1R and D2R; images are representative of the typical structures observed in each sample of triplicate experiments. Tile D1R yields many high aspect ratio lattices and curled ribbons which are consistent with the presence of tubular assemblies that open up as they land on mica. (A phenomenon commonly observed in DNA tubular assemblies (13).) The formation

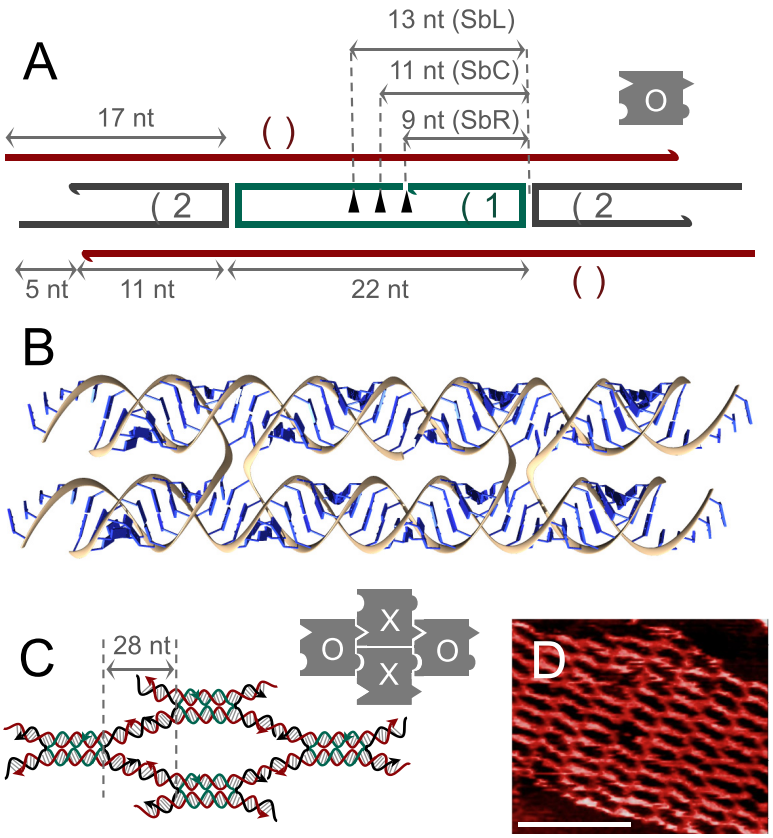

Figure 1. Design of DX RNA tiles (**A**) Schematic of DX RNA tile (29) and tile abstraction (gray). We tested tiles where the nick in strand Sb can be centered (SbC) or shifted two bases to the right (SbR) or to the left (SbL) of the midpoint between crossovers. (**B**) Three-dimensional rendering of the DX RNA tile motif. (**C**) Expected lattice geometry, where tiles assemble in an alternate facing up (O-marked tile) and facing down (X-marked tile) pattern. (**D**) Example, AFM image of lattices obtained with tiles presenting a right-shifted nick (design D1R described in the text). Scalebar is 50 nm.

of tubular assemblies is consistent with our expectations based on earlier results by Ko *et al.*, (29). AFM imaging compresses these soft samples and the height difference between open (single-layer) and closed (double-layer) structures is 2.049 ± 0.269 nm, in agreement with the expected diameter of double helical RNA (2.3 nm) (Supplementary Figures S2 and 3, SI Section 4). TEM images (Supplementary Figure S14, SI Section 10) suggest that D1R tubular structures form in solution and that assembly is not mica-assisted (4).

We asked if aggregation of nanostructures in our images is promoted by the presence of magnesium cations in solution; we found that aggregation appears to decrease at lower $MgCl_2$ concentration, however the yield of assembly decreases as well (Supplementary Figure S9, SI Section 7). We then asked if tile concentration could have an effect on aggregation: at a 12.5 mM $MgCl_2$ concentration, we varied the annealed tile concentration between 50 nm and 0.5 μm, and we found that aggregation persists even at low annealing concentrations (Supplementary Figure S10, SI Section 8). Aggregation makes it difficult to measure length and width of ribbons and tubular structures, which often overlap and appear to branch. We selected AFM images of 10 isolated, partially closed, tubular structures from each of three separate assembly experiments and we measured an average length of 489 ± 140 nm and an average width of 46 ± 5 nm (Supplementary Figure S4). The longest isolated nanotube assembled from D1R tiles measured 1.03 μm, but several tubular assemblies exceeding 1 μm in length can be identified among overlapping structures (Figure 2B).

We further tested a one-pot protocol in which all strands are simultaneously transcribed in the appropriate buffer for 15 min, immediately heated to 70°C and cooled over 24 h (Figure 2D). This protocol has the advantage of avoiding laborious gel extractions that can cause loss and degradation of significant amounts of transcript. Abortive and elongated RNA molecules produced during the transcription reaction, and not eliminated by gel extraction (Supplementary Figure S5, SI Section S5) contribute to generating a 'noisy' assembly environment, where strands with incorrect length can promote formation of spurious assemblies. Despite the presence of these unwanted products, the one-pot protocol yields assemblies for both tile designs D1R (tubular assemblies) and D2R (flat lattices), as shown in Figure 2E and F. The size of D2R lattices largely exceeds that of the corresponding samples obtained with the gel-extraction protocol. Assembly of variant D1RE, which includes a single stranded overhang in strand S1a, was rapidly tested using the one-pot protocol; Supplementary Figure S22 shows AFM images of tile D1RE tubular assemblies which grow

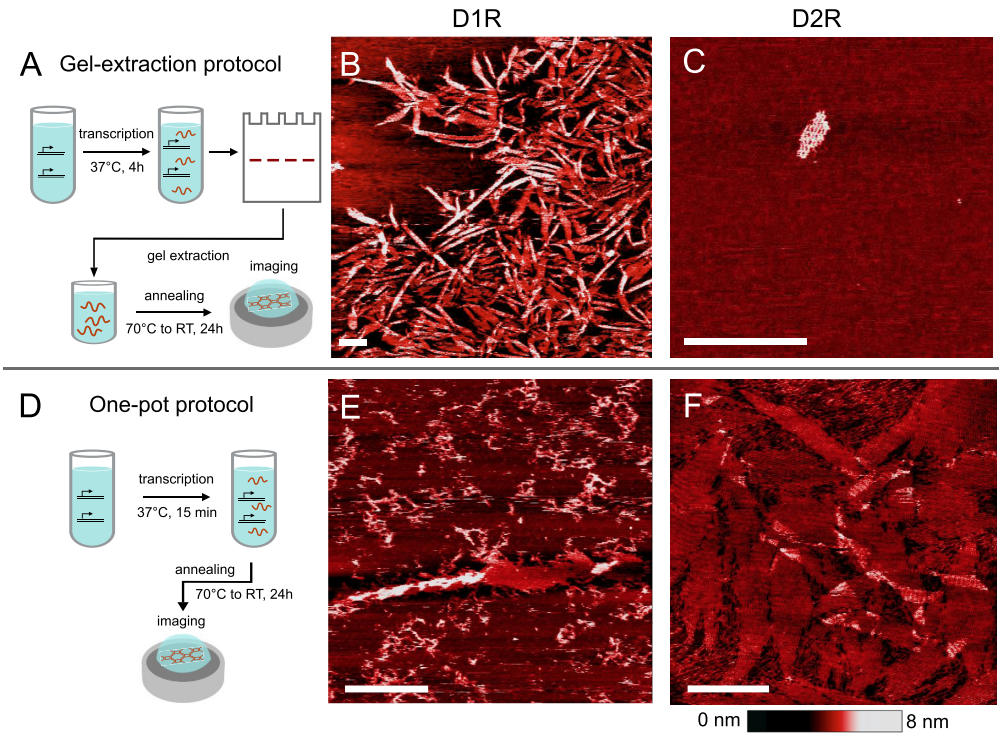

Figure 2. Assembly methods and results (**A**) Gel extraction and anneal protocol, showing templates with T7 promoter (black lines with bent arrows), RNA transcripts (red lines), and tile assembly. (**B**) Example, AFM image of assemblies obtained from tile D1R. (**C**) Representative image of small lattices obtained from tile D2R (additional images are in Supplementary Figure S20). (**D**) One-pot transcription and anneal protocol. (**E**) Example, AFM image of tubular structure produced from one-pot assembly of tiles D1R. (**F**) Lattices formed by one-pot assembly of tiles D2R. Scale bar: 250 nm.

up to 3 μm in length. The robust growth of this variant suggests that the presence of single stranded overhangs does not affect lattice assembly and appears to reduce aggregation; these overhangs may be used as domains for tile functionalization via chemical linking or base-pairing.

As can be seen in Figure 2B and Supplementary Figure S19 (SI Section 14), the yield of lattices varies significantly depending on the tile design. It is not possible to arrive at a rigorous quantitative assessment of lattice yield based on AFM or TEM images. But it is possible to qualitatively compare the yield of each tile variant based on the ease with which we could locate lattices under AFM. As we discuss in the next sections, the yield of lattices for each tile variant qualitatively depends not only on the sequence of strands and annealing protocol but also on subtle features of tile design such as the nick position.

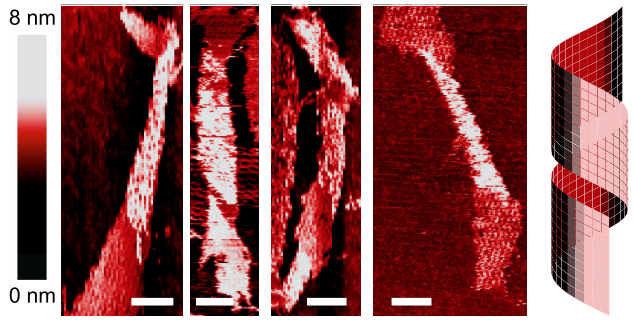

Figure 3. Example, AFM images of chiral tubular structures formed by D1R tiles. The chirality feature is presumably promoted by a combination of sequence content and tile geometry. A detailed discussion of handedness is provided in (SI section 13). Scale bar is 50 nm. Right: rendering of a left-handed chiral sheet as a guide to the eye.

Assembly morphology is sequence dependent

AFM images of structures produced from tile D1R reveal that many assemblies are tubular and chiral, as shown in the examples selected in Figure 3. The chirality can be interpreted in some cases as left-handed (Supplementary Figure S18, SI Section 13). Formation of tubular structures is unexpected given the face-up, face-down tile assembly pattern, which should yield flat lattices (Figure 1C), but consistent with the behavior of the hybrid DNA–RNA version of this motif (29). It is important to note that similar DNA DX tiles assemble into nanotubes due to the binding angle between adjacent tiles (13) and the tube axis is usually parallel to the helical axis. Rather, these RNA tubes form by coiling, where an array folds back to itself orthogonal to the helical axis. We observed formation of tubular assemblies exclusively in variants D1R and D1RE. We hypothesize that tile sequence content influences self-assembly morphology and may or may not promote chirality: comparison of AFM images of D1R and D2R tile assemblies, which only differ in tile sequence content, suggests that our hypothesis is valid, because tile D1R consistently yields tubular assem-

blies (with both assembly protocols), while tile D2R exclusively forms lattices (with both assembly protocols).

Nick position is critical for assembly

We further asked if chirality may also be related to the asymmetry of the nick position in strand Sb. In DNA duplexes, the presence of a nick leads to enhanced flexibility at the location of the nick (38). The position of the nick in the tile might affect how the stresses during self-assembly bend the tile double helical domains, which in turn would influence the curvature of lattices. To test this hypothesis, we modified strand Sb obtaining tiles with a central nick position (tiles D1C, D2C) or a left-shifted nick position (tiles D1L, D2L). (The different nick positions are shown in Figure 1A.) Tiles were then assembled according to the gel-extraction and one-pot protocols described earlier.

Only tile design D1R consistently yields chiral tubular structures, using either assembly protocol. Tile D2R only yields lattice and so do tiles D1L and D2L, which assemble into structures qualitatively similar to D2R (Supplementary Figure S20). In case of D1R (extracted and one-pot protocols), D2R (one-pot protocol), D2L (extracted protocol) and D2L (one-pot protocol), we could readily observe many structures on mica during AFM imaging. In case of D2R (extracted), D2L (extracted) and D1L (one-pot), we could only identify few lattices upon scanning many locations on mica under the AFM. No large structures assemble from tiles D1C and D2C, where the nick is in a central position in the core strand (Supplementary Figure S18). We do observe small, loose filaments in the AFM images of the D1C sample (Supplementary Figure S21). Using TEM, which gives much lower resolution, we were able to locate nanotubes for only the D1R (extracted) sample, as shown in Supplementary Figure S14. Clear TEM images could not be obtained for the one-pot annealed samples, due to the significant background noise.

Non-denaturing PAGE in Figure 4 A1–3 (see also SI section 9, Supplementary Figure S11) highlights differences between the complexes formed by the tile with a symmetric nick (D1C) and the ones with an asymmetric nick (D1R and D1L). Gel lanes 1 and 2 test the interactions between Sa and Sb strands. The Sa:Sb strands at 1:1 ratio are expected to run at a lower position (lane 1) compared to strands at 2:1 ratio (lane 2): this is because at 2:1 ratio two Sa strands should bind to one Sb strand. This expected result is verified for tiles D1R and D1L. But for tile D1C, the bands in both lane 4 and lane 5 run at the same position. This could be because the 2:1 ratio complex does not form well in the D1C design. A similar analysis was conducted on design D2 variants, however significant RNA degradation during annealing does not allow us to make conclusive observations on the results (Supplementary Figures S12 and 16). We also examined tile variants D1R*, D1C* and D1L*, from which we removed the sticky end domains (this tiles cannot multimerize). Non-denaturing PAGE of annealed tiles D1R* and D1L* yields single bands, as shown in Supplementary Figure S13; in contrast, D1C* samples yield two distinct bands, that suggest the formation of incompletely or incorrectly formed tiles. The lower band in lane 6 for D1C* sample corresponds in length to the Sa1 and SbC1 complex in lanes 4 and 5, which suggests that, during the anneal, this complex does not further self-assemble with Sc1 strand properly to form a tile.

In addition, agarose gel electrophoresis was used to compare multimerizing D1R, D1L and D1C tiles. Figure 4B shows that a significant fraction of annealed tile D1C runs closer to the band of the annealed control tile (D1C*) without sticky-ends (further details can be found in SI Section 11 and Supplementary Figure S15). This confirms that D1C monomers have the capacity to form some higher order complexes, which however do not appear to be as structured as those formed by tiles D1R and D1L.

These results overall indicate that nick position is an important parameter in the design of DX RNA tiles. Tiles with asymmetric nick positions (relative to the midpoint between the intra-tile crossovers) consistently form lattices, while the tiles with symmetric nicks do not form lattices. This is true for both D1 or D2 sequence design variants. To our knowledge, similar phenomena have not been observed in DNA tiles: for example, DAE-E tiles consistently form nanotubes even when the nick position in the central strand is varied, as long as the inter-tile distance is appropriately chosen (13,18,39). It is unclear why the centrally nicked designs fail to form lattices. Non-denaturing gels (Supplementary Figure S11) suggest misfolding of tiles with a central nick, which is potentially the reason why they do not form lattices. In our experiments, the nick position also affects the assembly morphology, with only D1R resulting in tubular structures and the other variants resulting in flat lattices. Further experiments, and computational modeling, are needed to quantitatively elucidate these phenomena.

Role of thermal annealing

In both assembly protocols, a heating temperature of at least 70°C is required for lattice formation (SI Section 6 and Supplementary Figures S6 and 7). Isothermal one-pot production of D1R and D2R tiles only results in tangled filaments (Supplementary Figure S8, SI Section 6.2). This outcome is not surprising, as thermal annealing is required for assembly of DNA DX tile motifs as well. One possibility is that secondary structure in individual strands creates a barrier to isothermal tile assembly (however, tile D2R strands were specifically designed to have no secondary structure at 37°C). Our results indicate that thermal annealing is essential for multi-stranded RNA tiles to form and bind. This limitation may be overcome by designing hierarchical assembly steps for tile components (11).

It is known that RNA degradation rates increase at high temperature and in the presence of Magnesium cations (40), which make the phosphodiester bonds more reactive: denaturing gels indicate that significant degradation occurs in all variants of design D2 upon annealing (Supplementary Figures S16, 17 and SI section 12), but not in D1 variants. We hypothesize that this difference may be due to different sequence content and secondary structure of individual strands, as both factors affect phosphodiester bond cleavage rates (41). We also note that one-pot produced D2R tiles, which are annealed in transcription mix, form very large lattices (Figure 2E), which indicates that degradation may also be influenced by the composition of the buffer.

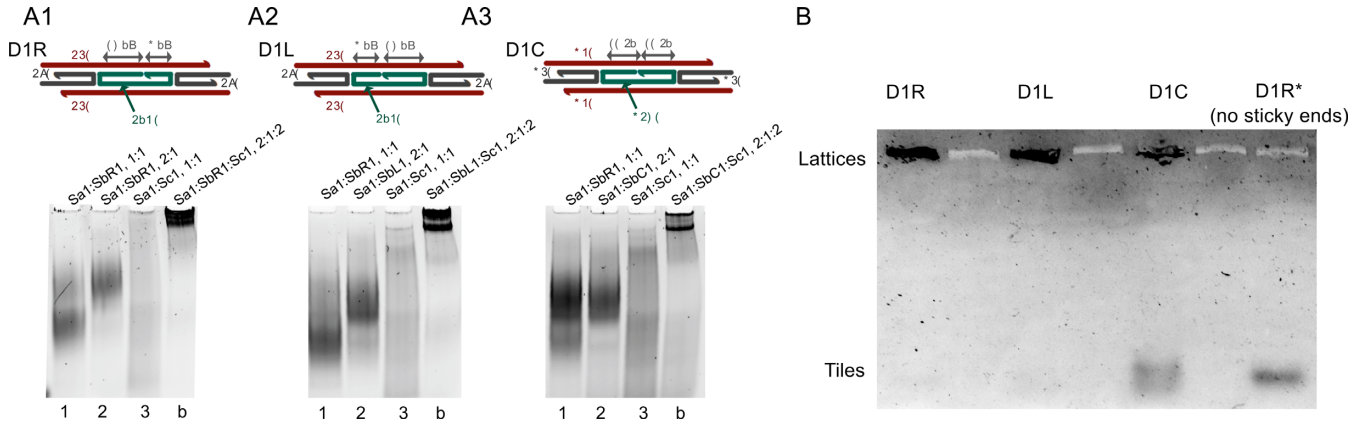

Figure 4. Gel analysis of assembling structures. Strands were gel extracted and annealed prior to loading them into the gel. (**A1**, **A2** and **A3**) Non-denaturing PAGE gels comparing complexes that form as part of tile variants D1R, D1L and D1C. Each lane was loaded with annealed strands as annotated on top of the gel. Ratio 1:1 indicates that both strands were annealed at a 1 μm concentration; ratio 2:1 indicates concentrations 1 μm : 500 nm; ratio 2:1:2 indicates concentrations 1 μm : 500nm : 1 μm. Bands forming in lanes 1 and 2 provide information on the formation of the core of the tile; Sa and Sb in stoichiometric amounts are expected to form smaller complexes relative to the case where Sa and Sb are in the 2:1 ratio required for tile formation. In variant D1C, the two cases are indistinguishable, which suggests improper formation of the tile core during annealing. (**B**) Agarose gel of annealed tile variants D1R, D1L and D1C, compared to non-multimerized annealed tile variant D1R*. A significant fraction of annealed tile D1C runs roughly as the D1R* control complex, indicating that D1C assemblies are not as robust as in the other variants.

DISCUSSION

We demonstrated that large RNA nanostructures can be built from multi-stranded DX tiles, a classical motif in DNA nanotechnology (32,42). In contrast with most methods to build large RNA assembled structures, which rely on conserved tertiary interactions such as kissing loops (10,43–45), these tiles assemble exclusively via double helical complementary domains whose sequence can be rationally determined within an ample design space.

Multi-stranded DX tiles qualitatively similar to our design were produced *in vivo* for colocalization of split fluorescent reporters and of metabolic pathway components (11,46), whose output was used as indirect evidence of co-transcriptional structure formation. These RNA tiles were originally designed by Delebecque *et al.* (11) and resemble a Double crossover, Anti-parallel with Odd number of half-turns between crossovers (DAO) DX tile (32,42). However, unlike the well characterized standard DNA DAO tile, this design includes unmatched bases and wobble base pairs. The presence of unmatched bases can make it difficult to control the angle between two interacting tiles because they become connected through unmatched floppy domains. As a result, it is difficult to enforce the formation of rigid lattices. In addition, Geary *et al.* (4) later demonstrated that a proper RNA DAO tile requires the two intra-tile crossover domains to have different length, due to the tilt of bases in (A-form) RNA. The design by Delebecque *et al.* does not take into account this requirement, therefore it is unlikely to yield a correct DAO tile (however, unmatched bases and wobble pairs may relax the spatial constraints posed by the incorrect length of intra-tile crossover domains). Unfortunately, the low resolution of AFM images provided in (11) makes it difficult to unequivocally determine whether the tessellated lattices or tubular structures are formed as desired.

Our multi-stranded structures were obtained with a protocol based on gel extraction as well as with a one-pot method where all strands are simultaneously transcribed and subsequently annealed. Previous studies (3,28,30) reported successful one-pot assembly of smaller multi-stranded RNA or RNA–DNA structures (up to 100 nm large and about 1000 bp). The one-pot method is less laborious and often produces structures of equal or larger size than those obtained with the gel-extraction method, despite the presence of well known phenomena of abortive and elongated (run-off) bacteriophage polymerase transcription (47–49). These processes generate undesired RNA strands presenting incorrect length and unknown folding. Abortive transcription is sequence dependent and can be mitigated using G-rich transcription initiation sequences (50). Elongated or 'run-off' transcription occurs in linear templates for transcription, and incorrect products with up to twice as long as the desired transcript can reach up to 70% of the total synthesized RNA (47). This phenomenon can be reduced by enforcing strong secondary structure at the 3′ end of the transcript (47,51). Another challenge in the one-pot protocol is posed by uneven transcription rates, which can cause stoichiometric imbalances among strands and reduce assembly yield. This issue can be straightforwardly mitigated by including promoter-appropriate transcription initiation sequences and balancing the template concentrations. The imposition of specific sequence content or secondary structure to ensure correct yield of products can, unfortunately, limit the nanostructure sequence design space. Feedback mechanisms that automatically increase or decrease the production of molecules depending on the downstream demand could also help balancing the transcription rates and the stoichiometry of components (52).

Thermal annealing is required for assembly of our structures. Isothermal assembly of multi-stranded RNA nanocubes was demonstrated using an assembly-activated light-up aptamer (3). However, our results indicate that co-transcriptional isothermal assembly for multi-stranded RNA DX tiles remains challenging (Supplementary Figure

S8). While multi-stranded, short components have the advantage of being less prone to local folding traps, a more successful route to isothermal assembly is given by long single-stranded tiles explicitly designed to take advantage of local folding (4). Another feasible approach to isothermal assembly is the design of strands that can exclusively assemble with an ordered sequence of reactions (11).

We find that the morphology of our assemblies is affected by sequence content. While the D1R tile sequence produced many chiral nanotube structures, the D2R tile sequences produced only lattices (with both assembly protocols). The sequence could directly affect the geometry of the tile and hence change the morphology of the assembly. Additionally, the degradation of RNA after annealing, seen in design D2 could also lead to changes in geometry of some of the tiles which in turn affects the morphology. Further, assembly is also affected by the position of the nick on the nicked helix of the tile, a design parameter that is not known to pose similar challenges in DNA self-assembly. Our gel assays suggest that the lack of lattice formation from centrally nicked tile variants could be due to misfolding of individual tiles.

It would be useful to predict the influence of sequence and nicks on RNA assembly using advanced computational modeling tools. Computational characterization of RNA nanostructure assembly, validated by experiments, has been successfully demonstrated (53). However, existing RNA sequence design toolboxes are not fully equipped for *de novo*, rational construction of large assemblies based on Holliday junction motifs, because they are either tailored to tecto-RNA elements (conserved sequences and tertiary interactions) (54,55) or to design reaction pathways (20) rather than nanostructures. Advances in rational design of RNA scaffolds will highly benefit from integrated software toolboxes akin to those available for DNA nanostructures (56–58). It is likely that coarse-grained simulations to predict the primary vibration modes of tile monomers (59) will help explaining emergent assembly patterns such as the chiral tubes we observed.

Large RNA lattices may be functionalized with protein-binding domains or small RNA molecules with therapeutic properties (siRNA, microRNA or antisense RNA) (24,60). While our lattices are not suited for *in vivo* isothermal assembly, they can be produced *in vitro* and transfected as scaffolding elements or drug delivery vectors, as we recently demonstrated (61). The spontaneous chirality of some of our assemblies makes them potentially useful as scaffolds for synthesis of optically active biomaterials (62), although additional investigation is required to quantitatively elucidate this feature.

SUPPLEMENTARY DATA

Supplementary Data are available at NAR Online.

ACKNOWLEDGEMENTS

The authors thank Paul W. K. Rothemund, Cody Geary, Kirill Afonin, Rebecca Schulman, Erik Winfree and Petr Šulc for helpful discussions and advise.

FUNDING

This research was primarily supported by U.S. National Science Foundation CAREER grant [DMR- 1450747], which supported J.M.S. and E.F. and provided most materials and supplies. H. K. K. S. was supported by U.S. Department of Energy grant [SC0010595]. Funding for open access charge: NSF Award [DMR-1450747].
Conflict of interest statement. None declared.

REFERENCES

1. Zhang,F., Nangreave,J., Liu,Y. and Yan,H. (2014) Structural DNA nanotechnology: state of the art and future perspective. *J.Am. Chem. Soc.*, **136**, 11198–11211.
2. Grabow,W.W. and Jaeger,L. (2014) RNA self-assembly and RNA nanotechnology. *Acc. Chem. Res.*, **47**, 1871–1880.
3. Afonin,K.A., Bindewald,E., Yaghoubian,A.J., Voss,N., Jacovetty,E., Shapiro,B.A. and Jaeger,L. (2010) *In vitro* assembly of cubic RNA-based scaffolds designed *in silico*. *Nat. Nanotechnol.*, **5**, 676–682.
4. Geary,C., Rothemund,P.W. and Andersen,E.S. (2014) A single-stranded architecture for cotranscriptional folding of RNA nanostructures. *Science*, **345**, 799–804.
5. Afonin,K.A., Kireeva,M., Grabow,W.W., Kashlev,M., Jaeger,L. and Shapiro,B.A. (2012) Co-transcriptional assembly of chemically modified RNA nanoparticles functionalized with siRNAs. *Nano Lett.*, **12**, 5192–5195.
6. Surana,S., Shenoy,A.R. and Krishnan,Y. (2015) Designing DNA nanodevices for compatibility with the immune system of higher organisms. *Nat. Nanotechnol.*, **10**, 741–747.
7. Grabow,W.W., Zakrevsky,P., Afonin,K.A., Chworos,A., Shapiro,B.A. and Jaeger,L. (2011) Self-assembling RNA nanorings based on RNAI/II inverse kissing complexes. *Nano Lett.*, **11**, 878–887.
8. Nasalean,L., Baudrey,S., Leontis,N.B. and Jaeger,L. (2006) Controlling RNA self-assembly to form filaments. *Nucleic Acids Res.*, **34**, 1381–1392.
9. Koyfman,A.Y., Braun,G., Magonov,S., Chworos,A., Reich,N.O. and Jaeger,L. (2005) Controlled spacing of cationic gold nanoparticles by nanocrown RNA. *J. Am. Chem. Soc.*, **127**, 11886–11887.
10. Chworos,A., Severcan,I., Koyfman,A.Y., Weinkam,P., Oroudjev,E., Hansma,H.G. and Jaeger,L. (2004) Building programmable jigsaw puzzles with RNA. *Science*, **306**, 2068–2072.
11. Delebecque,C.J., Lindner,A.B., Silver,P.A. and Aldaye,F.A. (2011) Organization of intracellular reactions with rationally designed RNA assemblies. *Science*, **333**, 470–474.
12. Shu,D., Moll,W.-D., Deng,Z., Mao,C. and Guo,P. (2004) Bottom-up assembly of RNA arrays and superstructures as potential parts in nanotechnology. *Nano Lett.*, **4**, 1717–1723.
13. Rothemund,P.W., Ekani-Nkodo,A., Papadakis,N., Kumar,A., Fygenson,D.K. and Winfree,E. (2004) Design and characterization of programmable DNA nanotubes. *J. Am. Chem. Soc.*, **126**, 16344–16352.
14. Zheng,J., Birktoft,J.J., Chen,Y., Wang,T., Sha,R., Constantinou,P.E., Ginell,S.L., Mao,C. and Seeman,N.C. (2009) From molecular to macroscopic via the rational design of a self-assembled 3D DNA crystal. *Nature*, **461**, 74–77.
15. Ke,Y., Ong,L.L., Sun,W., Song,J., Dong,M., Shih,W.M. and Yin,P. (2014) DNA brick crystals with prescribed depths. *Nat. Chem.*, **6**, 994–1002.
16. Ekani-Nkodo,A., Kumar,A. and Fygenson,D.K. (2004) Joining and scission in the self-assembly of nanotubes from DNA tiles. *Phys. Rev. Lett.*, **93**, 268301.
17. Yan,H., Park,S.H., Finkelstein,G., Reif,J.H. and LaBean,T.H. (2003) DNA-templated self-assembly of protein arrays and highly conductive nanowires. *Science*, **301**, 1882–1884.
18. Sharma,J., Chhabra,R., Cheng,A., Brownell,J., Liu,Y. and Yan,H. (2009) Control of self-assembly of DNA tubules through integration of gold nanoparticles. *Science*, **323**, 112–116.

19. Rothemund,P. W.K., Papadakis,N. and Winfree,E. (2004) Algorithmic self-assembly of DNA sierpinski triangles. *PLOS Biol.*, **2**, 424–436.
20. Zadeh,J.N., Steenberg,C.D., Bois,J.S., Wolfe,B.R., Pierce,M.B., Khan,A.R., Dirks,R.M. and Pierce,N.A. (2011) NUPACK: analysis of nucleic acid systems. *J. Comput. Chem.*, **32**, 170–173.
21. Markham,N.R. and Zuker,M. (2008) UNAFold software for nucleic acid folding and hybridization. *Methods Mol. Biol.*, **453**, 3–31.
22. Leontis,N.B., Lescoute,A. and Westhof,E. (2006) The building blocks and motifs of RNA architecture. *Curr. Opin. Struct. Biol.*, **16**, 279–287.
23. Guo,P., Zhang,C., Chen,C., Garver,K. and Trottier,M. (1998) Inter-RNA interaction of phage φ29 pRNA to form a hexameric complex for viral DNA transportation. *Mol. Cell*, **2**, 149–155.
24. Sharma,A., Haque,F., Pi,F., Shlyakhtenko,L.S., Evers,B.M. and Guo,P. (2016) Controllable self-assembly of RNA dendrimers. *Nanomedicine*, **12**, 835–844.
25. Yurke,B. and Mills,A.P. Jr (2003) Using DNA to power nanostructures. *Genet. Program. Evolvable Mach.*, **4**, 111–122.
26. Zhang,D.Y., Hariadi,R.F., Choi,H.M. and Winfree,E. (2013) Integrating DNA strand-displacement circuitry with DNA tile self-assembly. *Nat. Commun.*, **4**, 1965.
27. Gerling,T., Wagenbauer,K.F., Neuner,A.M. and Dietz,H. (2015) Dynamic DNA devices and assemblies formed by shape-complementary, non–base pairing 3D components. *Science*, **347**, 1446–1452.
28. Yu,J., Liu,Z., Jiang,W., Wang,G. and Mao,C. (2015) *De novo* design of an RNA tile that self-assembles into a homo-octameric nanoprism. *Nat. Commun.*, **6**, 1–6.
29. Ko,S.H., Su,M., Zhang,C., Ribbe,A.E., Jiang,W. and Mao,C. (2010) Synergistic self-assembly of RNA and DNA molecules. *Nat. Chem.*, **2**, 1050–1055.
30. Wang,P., Ko,S.H., Tian,C., Hao,C. and Mao,C. (2013) RNA–DNA hybrid origami: folding of a long RNA single strand into complex nanostructures using short DNA helper strands. *Chem. Commun.*, **49**, 5462–5464.
31. Endo,M., Takeuchi,Y., Emura,T., Hidaka,K. and Sugiyama,H. (2014) Preparation of chemically modified RNA origami nanostructures. *Chemistry*, **20**, 15330–15333.
32. Fu,T. and Seeman,N. (1993) DNA double-crossover molecules. *Biochemistry*, **32**, 3211–3220.
33. Pettersen,E.F., Goddard,T.D., Huang,C.C., Couch,G.S., Greenblatt,D.M., Meng,E.C. and Ferrin,T.E. (2004) UCSF Chimera: a visualization system for exploratory research and analysis. *J. Comput. Chem.*, **25**, 1605–1612.
34. Seeman,N.C. (1990) *De novo* design of sequences for nucleic acid structural engineering. *J. Biomol. Struct. Dyn.*, **8**, 573–581.
35. Winfree,E. (2004) http://centrosome.caltech.edu/DNAdesign/.
36. Dirks,R.M., Lin,M., Winfree,E. and Pierce,N.A. (2004) Paradigms for computational nucleic acid design. *Nucleic Acids Res.*, **32**, 1392–1403.
37. Hofacker,I.L. (2003) Vienna RNA secondary structure server. *Nucleic Acids Res.*, **31**, 3429–3431.
38. Protozanova,E., Yakovchuk,P. and Frank-Kamenetskii,M.D. (2004) Stacked–unstacked equilibrium at the nick site of DNA. *J. Mol. Biol.*, **342**, 775–785.
39. Mitchell,J.C., Harris,J.R., Malo,J., Bath,J. and Turberfield,A.J. (2004) Self-assembly of chiral DNA nanotubes. *J. Am. Chem. Soc.*, **126**, 16342–16343.
40. Li,Y. and Breaker,R.R. (1999) Kinetics of RNA degradation by specific base catalysis of transesterification involving the 2'-hydroxyl group. *J. Am. Chem. Soc.*, **121**, 5364–5372.
41. Kaukinen,U., Lyytikäinen,S., Mikkola,S. and Lönnberg,H. (2002) The reactivity of phosphodiester bonds within linear single-stranded oligoribonucleotides is strongly dependent on the base sequence. *Nucleic Acids Res.*, **30**, 468–474.
42. Seeman,N.C. (1982) Nucleic acid junctions and lattices. *J. Theor. Biol.*, **99**, 237–247.
43. Jaeger,L., Westhof,E. and Leontis,N.B. (2001) TectoRNA: modular assembly units for the construction of RNA nano-objects. *Nucleic Acids Res.*, **29**, 455–463.
44. Nasalean,L., Baudrey,S., Leontis,N.B. and Jaeger,L. (2006) Controlling RNA self-assembly to form filaments. *Nucleic Acids Res.*, **34**, 1381–1392.
45. Severcan,I., Geary,C., Chworos,A., Voss,N., Jacovetty,E. and Jaeger,L. (2010) A polyhedron made of tRNAs. *Nat. cCem.*, **2**, 772–779.
46. Sachdeva,G., Garg,A., Godding,D., Way,J.C. and Silver,P.A. (2014) *In vivo* co-localization of enzymes on RNA scaffolds increases metabolic production in a geometrically dependent manner. *Nucleic Acids Res.*, **42**, 9493–9503.
47. Triana-Alonso,F.J., Dabrowski,M., Wadzack,J. and Nierhaus,K.H. (1995) Self-coded 3'-extension of run-off transcripts produces aberrant products during *in vitro* transcription with T7 RNA polymerase. *J. Biol. Chem.*, **270**, 6298–6307.
48. Hsu,L.M., Vo,N.V., Kane,C.M. and Chamberlin,M.J. (2003) *In vitro* studies of transcript initiation by Escherichia coli RNA polymerase. 1. RNA chain initiation, abortive initiation, and promoter escape at three bacteriophage promoters. *Biochemistry*, **42**, 3777–3786.
49. Goldman,S.R., Ebright,R.H. and Nickels,B.E. (2009) Direct detection of abortive RNA transcripts *in vivo*. *Science*, **324**, 927–928.
50. Martin,C.T., Muller,D.K. and Coleman,J.E. (1988) Processivity in early stages of transcription by T7 RNA polymerase. *Biochemistry*, **27**, 3966–3974.
51. Kim,J., White,K.S. and Winfree,E. (2006) Construction of an *in vitro* bistable circuit from synthetic transcriptional switches. *Mol. Sys. Biol.*, **1**, 68.
52. Franco,E., Giordano,G., Forsberg,P.-O. and Murray,R.M. (2014) Negative autoregulation matches production and demand in synthetic transcriptional networks. *ACS Syn. Biol.*, **3**, 589–599.
53. Afonin,K.A., Kasprzak,W., Bindewald,E., Puppala,P.S., Diehl,A.R., Hall,K.T., Kim,T.J., Zimmermann,M.T., Jernigan,R.L., Jaeger,L. *et al.* (2014) Computational and experimental characterization of RNA cubic nanoscaffolds. *Methods*, **67**, 256–265.
54. Bindewald,E., Hayes,R., Yingling,Y.G., Kasprzak,W. and Shapiro,B.A. (2008) RNAJunction: a database of RNA junctions and kissing loops for three-dimensional structural analysis and nanodesign. *Nucleic Acids Res.*, **36**(suppl. 1), D392–D397.
55. Martinez,H.M., Maizel,J.V. Jr and Shapiro,B.A. (2008) RNA2D3D: a program for generating, viewing, and comparing 3-dimensional models of RNA. *J. Biomol. Struct. Dyn.*, **25**, 669–683.
56. Williams,S., Lund,K., Lin,C., Wonka,P., Lindsay,S. and Yan,H. (2009) Tiamat: a three-dimensional editing tool for complex DNA structures. In: Goel,A, Simmel,FC and Sosík,P (eds). *DNA Computing, DNA 2008. Lecture Notes in Computer Science*. Springer, Berlin, Heidelberg, Vol. **5347**, pp. 90–101.
57. Andersen,E.S., Dong,M., Nielsen,M.M., Jahn,K., Lind-Thomsen,A., Mamdouh,W., Gothelf,K.V., Besenbacher,F. and Kjems,J. (2008) DNA origami design of dolphin-shaped structures with flexible tails. *ACS Nano*, **2**, 1213–1218.
58. Douglas,S.M., Marblestone,A.H., Teerapittayanon,S., Vazquez,A., Church,G.M. and Shih,W.M. (2009) Rapid prototyping of 3D DNA-origami shapes with caDNAno. *Nucleic Acids Res.*, **37**, 5001–5006.
59. Qian,P., Seo,S., Kim,J., Kim,S., Lim,B.S., Liu,W.K., Kim,B.J., LaBean,T.H., Park,S.H. and Kim,M.K. (2012) DNA nanotube formation based on normal mode analysis. *Nanotechnology*, **23**, 105704.
60. Afonin,K.A., Viard,M., Kagiampakis,I., Case,C.L., Dobrovolskaia,M.A., Hofmann,J., Vrzak,A., Kireeva,M., Kasprzak,W.K., KewalRamani,V.N. *et al.* (2014) Triggering of RNA interference with RNA–RNA, RNA–DNA, and DNA–RNA nanoparticles. *ACS Nano*, **9**, 251–259.
61. Stewart,J.M., Viard,M., Subramanian,H.K., Roark,B.K., Afonin,K.A. and Franco,E. (2016) Programmable RNA microstructures for coordinated delivery of siRNAs. *Nanoscale*, **8**, 17542–17550.
62. Kuzyk,A., Schreiber,R., Fan,Z., Pardatscher,G., Roller,E.M., Hogele,A., Simmel,F.C., Govorov,A.O. and Liedl,T. (2012) DNA-based self-assembly of chiral plasmonic nanostructures with tailored optical response. *Nature*, **483**, 311–314.